ELSEVIER

International Journal of Heat and Fluid Flow 22 (2001) 561–570

International Journal of HEAT AND FLUID FLOW

www.elsevier.com/locate/ijhff

Bénard cells in fluid-saturated porous enclosures with lateral cooling

E. Bilgen [a,*], M. Mbaye [b]

[a] *Ecole Polytechnique, University of Montreal, C.P. 6079, 'Centre Ville', Montreal, Que., Canada H3C 3A7*
[b] *Shape Casting Platform, Alcoa Technical Center, 100 Technical Drive, Alcoa Center, PA 15069-0001, USA*

Received 13 September 2000; accepted 19 February 2001

Abstract

The development of Bénard cells is studied in fluid-saturated porous enclosures whose bottom (warm) and top (cold) walls are isothermal, and its lateral walls are cooled. To model the laminar natural convection, the Darcy law with the Boussinesq approximation is used. The finite difference method is used to solve the resulting differential equations. The energy equation is solved with the implicit scheme using the ADI method and the stream function equation using the SOR method. The results are analyzed in terms of the Darcy–Rayleigh number *Ra*, the Biot number *Bi* and the initial conditions. The results show that two branches exist that are related to the Darcy–Rayleigh and Biot numbers. The fluid remains stationary below a certain value of the Darcy–Rayleigh number, i.e., the state of rest. Two convective solution branches bifurcate from the zero solution in the direction of increasing *Ra*. If *Ra* is increased further, the solutions at $Ra \simeq 390$ become unstable with respect to oscillatory disturbances.

1. Introduction

In recent years a great deal of interest has focused on the knowledge of the natural convection mechanism in a fluid saturated porous medium. Studies have been made on different geometries and heating conditions. Especially, the transition between unicellular and multicellular convection has attracted attention. Moya and Ramos (1987) performed a numerical study of natural convection in a tilted rectangular cavity to demonstrate the existence of multiple steady-state solutions. Zhang (1992) studied the duality of solutions on natural convection in an inclined water-saturated porous cavity in the presence of density inversion. These studies focused on the influence of the tilt angle.

The convective instabilities of a horizontal porous layer heated from the below have been investigated by several authors (Combarnous and Bories (1975); Caltagirone (1975); Cheng (1978)). It is now well known that the onset of convection takes place at a critical Darcy–Rayleigh number, $Ra_c = 4\pi^2$. The forward bifurcation at $Ra = Ra_c$ implies the loss of stability for the conductive solution with velocity amplitude $V = 0$, and the emergence of two stable convective solutions for $Ra > Ra_c$ with a flow in either the clockwise or counterclockwise direction. If *Ra* is increased further, two-dimensional convection becomes oscillatory (Horne and O'Sullivan (1974); Caltagirone (1975)). To define the critical conditions for the onset of oscillatory convection, Horne and O'Sullivan (1974) observed that the flow displays a periodically oscillatory behavior in the unicellular mode at $Ra \leqslant 280$ while the corresponding multicellular solutions are steady. Caltagirone (1975) has performed a stability analysis based on a numerical study, which predicted the onset of oscillatory behavior at $Ra = 384 \pm 5$ for unicellular flow and at *Ra* between 800 and 1000 for bicellular convection in a square cell.

In a later study, Horne and O'Sullivan (1978) investigated the origin of the oscillatory regime and found that the oscillatory flow arises from the instability of thermal boundary layer on the heated bottom surface. Schubert and Straus (1979) performed a three-dimensional study and found that in a cube, unsteady convection starts when *Ra* exceeds a value between 300 and 320, similar to the unicellular two-dimensional flow in a square cavity. Another three-dimensional study was performed by Caltagirone et al. (1981) to enumerate various stable structures for different Rayleigh numbers ($Ra < 150$) and aspect ratios. The model, based on the application of Galerkin's method, has shown that for the same configuration, different stationary structures are developed according to the initial conditions.

A further increase of the Rayleigh number results in discrete flow transitions that increase the spatial as well as temporal complexity of the flow and temperature field, finally leading to turbulent flow. For instance, the flow field may undergo the following sequence of changes: steady state → periodic → quasi-periodic → steady state. In a three-dimensional rectangular cavity filled with fluid media Mukutmoni and Yang (1995) found that when the Rayleigh number is increased, the rather counter-intuitive reversion to steady state from quasi-periodicity, which is steady state → periodic → quasi-periodic → steady state, is due to spatial changes in the

* Corresponding author. Tel.: +1-514-340-4711 ext. 4579; fax: +1-514-340-5917.
E-mail address: bilgen@meca.polymtl.ca (E. Bilgen).

0142-727X/01/$ - see front matter
PII: S0142-727X(01)00107-2

Notation

A	aspect ratio ($= H/L$)
Bi	Biot number ($= h_a L/k$)
c	heat capacity (J kg^{-1} K^{-1})
g	gravitational acceleration (m s^{-2})
H	height of the cavity (m)
h	convective heat transfer coefficient (W m^{-2} K^{-1})
K	permeability (m^2)
k	thermal conductivity of the fluid filled medium (W m^{-1} K^{-1})
L	width of the cavity (m)
Nu	Nusselt number ($= hL/k$)
p'	pressure (Pa)
Ra	Darcy–Rayleigh number ($= g\beta\Delta T' KL/(v\alpha)$)
T'	temperature (K)
t	time (s)
u', v'	fluid velocity in x, y direction (m s^{-1})
u, v	dimensionless fluid velocity ($= uL/\alpha, vL/\alpha$)
x', y'	Cartesian coordinates (m)
x, y	dimensionless coordinates in x, y direction ($= x/L, y/L$)

Greeks

α	thermal diffusivity ($= k/(\rho c_p)$) (m^2 s^{-1})
β	thermal expansion coefficient of fluid (K^{-1})
$\Delta T'$	temperature difference ($= T'_1 - T'_2$)
T	dimensionless temperature ($= (T' - T'_2)/\Delta T'$)
μ	dynamic viscosity (kg m^{-1} s^{-1})
v	kinematic viscosity (m^2 s^{-1})
ρ	fluid density (kg m^{-3})
τ	dimensionless time ($= t/(\sigma L^2/\alpha)$)
ϕ	porosity
ψ'	stream function (m^2 s^{-1})
ψ	dimensionless stream function ($= \psi'/\alpha$)
σ	ratio of heat capacities of fluid saturated porous medium and fluid

Subscript

a	atmospheric
b	bottom
f	fluid medium
l	left
p	fluid saturated porous medium
r	right
t	top
0	reference

Superscript

$'$	dimensional variables

mean velocity and temperature fields that accompany the bifurcation.

Graham and Steen (1994) studied the beginning of the high Rayleigh number regime, where convection is dominated by buoyancy and molecular diffusion plays little part in the bulk of the flow. Their main result is the observation and study of instabilities that lead to deviations from the scaling relations. As the Rayleigh number increases further, the flow undergoes instabilities that lead to "bubbles" in parameter space of quasi-periodic flow and eventually to weakly chaotic flow.

Others have focused on the influence of the Rayleigh number. Caltagirone (1975) has studied thermoconvective instabilities in a horizontal porous layer. His analysis, based on the Galerkin method, enables one to determine the critical conditions of stability for the pure conduction ($Ra \leqslant 4\pi^2$), the regime of stable convection ($Ra \leqslant 384$) and the fluctuating regime ($Ra > 384$) for a square cavity. These results agree with those obtained by Bories (1970) and Combarnous (1970). Further results can be found for high Rayleigh numbers in the work of Caltagirone and Fabrie (1989).

It is noted that all the above-mentioned studies have been done on a horizontal porous layer with the following physical boundary conditions: isothermal bottom (warm) and top (cold) walls, and adiabatic lateral walls. Yet in all the applications, the assumption of adiabatic (or constant temperature) lateral walls is a simplification of more complex problems. In reality, in most of the practical situations the lateral walls are non-adiabatic and often non-isothermal. In fact, the literature review shows that, the condition of non-adiabatic lateral walls has not been considered, and its influence on the bifurcation phenomena has not been studied.

The purpose of the present study is to contribute to the understanding of the bifurcation phenomena observed in a horizontal fluid-saturated porous layer with non-adiabatic lateral walls. In particular, we will consider a saturated porous layer bounded by two horizontal plates separated by a height H and subjected to a temperature gradient $\Delta T'$, and two vertical walls separated by a distance L and cooled by convective heat transfer to the surrounding air. The convective cooling at these boundaries may be described by

$$-k\frac{\partial T'}{\partial x'} = h_a(T' - T'_0).$$

2. Mathematical formulation

Fig. 1 shows schematically the physical situation and the coordinate system.

It is assumed that the fluid is incompressible, the viscous dissipation is negligible and all thermophysical properties are constant, except for the density variations in the buoyancy term as modeled using the Boussinesq approximation. By using the Darcy model for laminar and two-dimensional flow, the governing equations are:

$$\rho = \rho_0[1 - \beta(T' - T'_0)], \tag{1}$$

$$\nabla \cdot \vec{V}' = 0, \tag{2}$$

$$-\nabla p' - \frac{\mu}{K}\vec{V}' + \rho\vec{g} = 0, \tag{3}$$

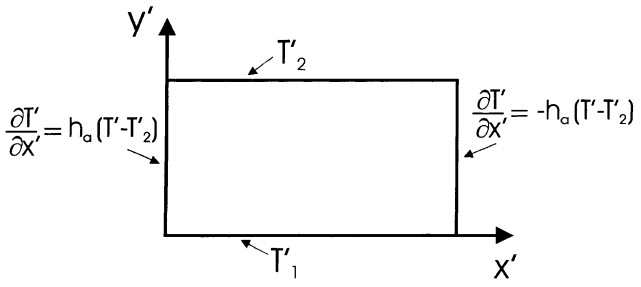

Fig. 1. Physical model and system coordinate.

Table 1
Numerical results[a]

	Caltagirone (1975)		Schubert and Straus (1979)		Present	
Ra	*Nu*	ψ_{max}	*Nu*	ψ_{max}	*Nu*	ψ_{max}
50	1.450	2.112	–	–	1.443	2.099
100	2.651	5.377	2.651	–	2.631	5.359
200	3.813	8.942	3.808	–	3.784	8.931
250	4.199	10.253	–	–	4.167	10.244
300	4.523	11.405	4.514	–	4.487	11.394

[a] Nusselt number *Nu*, maximum value ψ_{max} of the stream function for different values of the Rayleigh number *Ra* and of the aspect ratio $A = 1$.

$$(\rho c)_p \frac{\partial T'}{\partial t} + (\rho c)_f \nabla \cdot \vec{V}' T' = \nabla \cdot k_p \nabla T', \tag{4}$$

where $\vec{V}'$ is the filtration velocity.

The boundary conditions are:

$$\begin{aligned}
&x' = 0 \quad k\frac{\partial T'}{\partial x'} = +h_a(T' - T_2') \quad \psi' = 0,\\
&x' = L \quad k\frac{\partial T'}{\partial x'} = -h_a(T' - T_2') \quad \psi' = 0,\\
&y' = 0 \quad T' = T_1', \quad \psi' = 0,\\
&y' = H \quad T' = T_2', \quad \psi' = 0.
\end{aligned} \tag{5}$$

The above equations may be made dimensionless by using

$$\begin{aligned}
&(x, y) = \frac{(x', y')}{L} \quad (u, v) = \frac{(u', v')L}{\alpha},\\
&\psi = \psi'/\alpha \quad \tau = \frac{t\alpha}{\sigma L^2},\\
&T = \frac{T' - T_2'}{\Delta T'} \quad \Delta T' = T_1' - T_2',\\
&u = \frac{\partial \psi}{\partial y} \quad v = -\frac{\partial \psi}{\partial x},
\end{aligned}$$

where T_1' and T_2' are the temperature of the bottom and top walls and it is arbitrarily assumed that $T_2' = T_0'$.

As we are considering a two-dimensional problem, it is convenient to introduce the stream function ψ defined by $\psi_x = -v$, $\psi_y = u$ so that the continuity equation is satisfied automatically. The governing equations for the temperature and flow fields may be expressed in the following dimensionless form:

$$\nabla^2 \psi = -Ra \frac{\partial T}{\partial x}, \tag{6}$$

$$\frac{\partial T}{\partial \tau} + \frac{\partial \psi}{\partial y}\frac{\partial T}{\partial x} - \frac{\partial \psi}{\partial x}\frac{\partial T}{\partial y} = \nabla^2 T \tag{7}$$

with the boundary conditions

$$\begin{aligned}
&x = 0 \quad \frac{\partial T}{\partial x} = +BiT \quad \psi = 0,\\
&x = 1 \quad \frac{\partial T}{\partial x} = -BiT \quad \psi = 0,\\
&y = 0 \quad T = 1, \quad \psi = 0,\\
&y = A \quad T = 0, \quad \psi = 0.
\end{aligned} \tag{8}$$

From the above equations, it appears that the problem is governed by the following parameters: the Darcy–Rayleigh number *Ra*, the Biot number *Bi*, the aspect ratio *A* and the initial conditions.

The average Nusselt number at the bottom and top walls is

$$Nu_{b,t} = -\int_0^1 \left.\frac{\partial T}{\partial y}\right|_{y=0,A} \mathrm{d}x \tag{9}$$

and at the cooled lateral walls

$$Nu_{l,r} = -\frac{1}{A}\int_0^A \left.\frac{\partial T}{\partial x}\right|_{x=0,1} \mathrm{d}y. \tag{10}$$

The heat flux $(\partial T/\partial x_i)(x_i = x, y)$ is calculated by a Taylor series expansion with four points. For a good accuracy, the integration was evaluated by a combination of the Simpson's 1/3 and 3/8 rules for an odd number of intervals and only 1/3 rule for an even number of intervals.

3. Numerical method

Eqs. (6) and (7) describing the flow and temperature fields of this problem were solved numerically using a finite-difference discretization procedure. Central-difference formulae were used for all spatial derivative terms. A modified alternate direction implicit procedure was used to solve the temperature equation. The finite-difference form of energy equation was written in conservative form for the convective terms to preserve the conservative form property (Roache, 1982). The stream function equation was solved by a successive over-relaxation method. The velocity field was obtained by integration of the stream function.

The boundary conditions for the energy equation in differential form may be written in finite difference form employing one-sided differences or a fictitious grid point outside the region. However, a greater accuracy and often more flexibility is obtained by considering the grid control volume which ensures, for a surface grid point, the energy and mass conservations. The energy equation (7) is integrated in the first control volume of the boundary and the final equation after applying the divergence theorem as

$$\frac{\partial}{\partial t}\int_{\mathscr{V}} T \mathrm{d}\mathscr{V} + \int_S \vec{V} T \cdot \overrightarrow{\mathrm{d}S} = \int_S \nabla T \cdot \overrightarrow{\mathrm{d}S}, \tag{11}$$

where $\mathscr{V}$ and *S* are the volume and the surface of an element, respectively.

To start a solution, an initial sinusoidal perturbation of stream function field or a well-established flow for a given *Ra* number is introduced to drive the solution. The iterative convergence of the stream function and temperature is checked by comparing two successive iterations *n* and $n+1$ at any node

$$\max\left\{\left|\frac{\psi^{n+1} - \psi^n}{\psi^n}\right|, \left|\frac{T^{n+1} - T^n}{T^n}\right|\right\} < 10^{-5}. \tag{12}$$

The steady state was reached when the maximum of the fractional changes in ψ_{max}, ψ_{min} and in the bottom Nusselt number Nu_b between time steps of (k) and $(k-10)$ are expressed as

Table 2
Initial conditions, Ra and Bi range, number of cells and circulation mode and reference to figures for various cases[a]

Initial conditions	Condition of computation	No. cells and circulation mode	Remark	Figure
From rest state	$Ra = 0 \rightarrow 100$, $Bi = 0$	1 cell N	1 cell at $Ra \geqslant 4\pi^2$	2
Solution from higher Ra	$Ra = 100 \rightarrow 0$, $Bi = 1 \rightarrow 5$	1 cell N	SB	
	$Ra = 100 \rightarrow 0$, $Bi = 0$	1 cell N	N-SB stable at $Ra \leqslant 80$	
1 or 2 cells N				
2 cells, $Ra = 100$, $Bi = 1$	$Ra = 100 \rightarrow 0$, $Bi = 1$	2 cells N	SB	
1 cell, $Ra = 100$, $Bi = 0$	$Ra = 100 \rightarrow 0$, $Bi = 0.5$	1 cell N	N-SB	
1 cell, $Ra = 100$,$Bi = 0$	$Ra = 100 \rightarrow 0$	1 cell N	N-SB	
1 cell N	$Ra = 100 \rightarrow 0$, $Bi = 0 \rightarrow 0.7$	1 cell N	N-SB	3
$Ra = 400$, $Bi = 0$	$Ra = 100 \rightarrow 0$, $Bi = 0.8 \rightarrow 1.1$	1 cell N	SB	3
	$Ra = 400 \rightarrow 0$, $Bi = 0 \rightarrow 1$	1 cell N	oscillating cell at $Ra \geqslant 370$	4
2 cells A-N				6, 7
(a) $Ra = 100$, $Bi = 0$	$Bi \leqslant 0.8$	A-N		
	$Bi > 0.8$	N		
(b) $Ra = 100$, $Bi = 0.2$	$Bi \leqslant 0.4$	1 cell A-N		
	$0.4 < Bi \leqslant 0.8$	2 cells N		
	$Bi > 0.8$	2 cells N		
(c) $Ra = 250$, $Bi = 0$	$Bi \leqslant 0.95$	2 cells A-N		
	$Bi > 0.95$	2 cells N		
A-N $Ra = 250$, $Bi = 0$	$Ra = 250$, $Bi = 0.95$	4 cells $\rightarrow$ 2 cells A-N $\rightarrow$ N		8,9
2 cells A-N $Ra = 100$, $Bi = 0.2$	$Bi \leqslant 0.4$	N		
	$0.4 < Bi \leqslant 0.8$	A-N		
	$0.8 < Bi \leqslant 1.1$	N		
2 cells A-N $Ra = 250$, $Bi = 0$	Ra $0 \rightleftharpoons 500$ $Bi = 0.1 \rightarrow 1$			10,11
	$Bi = 0.1$, $Ra > 40$	2 cells A-N	UB	
	$Bi = 0.1$, $70 < Ra < 80$	1 cell A-N		
	$Bi = 0.1$, $Ra > 80$	2 cells A-N		
	$Bi = 0.1$, $Ra > 70$	2 cells A-N	LB	
	$Bi = 0.2$, $Ra > 60$	2 cells A-N	UB	
	$Bi = 0.2$, $60 < Ra < 70$	1 cell A-N		
	$Bi = 0.2$, $Ra < 80$	2 cells A-N		
	$Bi = 0.2$, $Ra > 40$	2 cells A-N	LB	
	$Bi = 0.2$, $60 < Ra < 70$	1 cell A-N		
	$Bi = 0.2$, $Ra < 80$	2 cells A-N		
	$Bi = 0.5$, $Ra < 80$	2 cells A-N	SB	
	$Bi = 0.5$, $80 < Ra < 90$	1 cell A-N		
	$Bi = 0.5$, $Ra < 90$	2 cells A-N		
	$Bi = 1$, $0 < Ra \leqslant 250$	2 cells A-N	SB	
2 cells A-N $Ra = 100 \rightarrow 0$ $Bi = 1$	$Ra = 100 \rightarrow 0$, $Bi = 0 \rightarrow 1$			
2 cells A-N $Ra = 250$, $Bi = 0$	$Ra = 250 \rightarrow 0$, $Bi = 0.1$			
	$Ra = 0 \rightarrow 250$, $Bi = 0.1$			
	$Ra < 50$	2 cells A-N		
	$50 \leqslant Ra < 60$	1 cell A-N		
	$Ra \geqslant 80$	2 cells A-N		
2 cells A-N $Ra = 0 \rightarrow 250$, $Bi = 0.2$	$Ra = 250 \rightarrow 0$, $Bi = 0.2$			
	$Ra < 50$	2 cells A-N		
	$50 \leqslant Ra < 60$	1 cell A-N		
	$70 \geqslant Ra \leqslant 250$	2 cells A-N		
2 cells A-N $Ra = 250$, $Bi = 0$	$Ra = 250 \rightarrow 0$, $Bi = 0.5$			
	$Ra = 0 \rightarrow 250$, $Bi = 0.5$			
	$Ra \leqslant 80$	2 cells N		
	$90 \geqslant Ra \leqslant 200$	2 cells A-N		

Table 2 (Continued)

Initial conditions	Condition of computation	No. cells and circulation mode	Remark	Figure
2 cells A-N	$Ra = 250 \rightarrow 0$, $Bi = 1$	N		
$Ra = 250$, $Bi = 0$	$Ra = 0 \rightarrow 250$, $Bi = 1$	N		
2 cells A-N				12
$Ra = 500$, $Bi = 0$	$Ra = 0 \rightarrow 500$, $Bi = 0$			
	$40 < Ra < 500$	2 cells N	oscillation at $Ra > 440$	
	$Ra = 500 \rightarrow 0$, $Bi = 0$	$2 \rightarrow 1 \rightarrow 2$ cells	N-SB	
	$Ra > 70$	2 cells N	LB	
	$Ra = 0 \rightarrow 500$, $Bi = 1$	2 cells A-N	SB	
	$Ra = 500 \rightarrow 0$, $Bi = 1$		SB	
	$Ra < 260$	2 cells A-N		
	$260 < Ra < 270$	1 cell A-N		
	$Ra > 270$	4 cells N		

[a] N = Natural circulation, A-N = Anti-Natural circulation, SB = Symmetric Branch, N-SB = Non-Symmetric Branch, UB = Upper Branch, LB = Lower Branch.

$$\max\left\{\left|\frac{\psi^{k}_{\max}-\psi^{k-10}_{\max}}{\psi^{k-10}_{\max}}\right|,\left|\frac{\psi^{k}_{\min}-\psi^{k-10}_{\min}}{\psi^{k-10}_{\min}}\right|,\left|\frac{Nu^{k}_{b}-Nu^{k-10}_{b}}{Nu^{k-10}_{b}}\right|\right\} < 10^{-10}. \quad (13)$$

To achieve the desired accuracy and the numerical stability, a small time step ($\Delta\tau = 10^{-3}$–10^{-4}) was used. The discretization scheme of the governing equations is second-order accurate. The uniform mesh sizes were used in both x and y directions, and were varied from 41×41 to 81×81 depending on the strength of convection. Independence of solution on the grid size was studied for various cases. For instance, with $A = 1$, for $Ra = 100$ and $Bi = 0.1$, five different grid sizes from 21×21 to 101×101 were tried. The results showed that grid independence was achieved above 41×41 showing negligible differences in ψ_{ext} (0.01%) and the same multiple steady states were produced. Caltagirone (1975) has used 24×24 to 48×48 and the corresponding range of Ra was from 0 to 2000. A test of accuracy of the present numerical program was made by comparing with the results reported by Caltagirone (1975) and Schubert and Straus (1979) for the limiting case $Bi = 0$. Table 1 shows an excellent agreement with less than 1% deviation.

4. Results and discussion

Numerical experiments were carried out for $0 \leqslant Ra \leqslant 500$, $0 \leqslant Bi \leqslant 5$ and for the aspect ratio of $A = 1$, with various initial conditions. For most of the experiments, the data were obtained by increasing or decreasing the Darcy–Rayleigh number, Ra, by using an increment of 10, from 0 to 100 or from 100 to 0, respectively, and some Ra up to 500. The initial conditions for the first run were the rest state and those of the lower branch from steady-state solutions at higher Ra values. All subsequent runs were performed with initial conditions at the previous state. The initial conditions and observations for various cases are presented in Table 2.

A multiplicity of steady-state solutions is manifested in the present situation. This is characterized by the flow in the cavity, which will be identified by a variable stream function defined as

$$\psi_{ext} = \pm \max|\psi(x,y)|, \quad (14)$$

where the positive and negative signs correspond to counterclockwise and clockwise circulation, respectively.

If the multiple states are stable to small perturbations, they may exist in practice as shown experimentally for flow in natural convection loops (see, for example, Bau and Torrance (1981)). Usually, initial conditions determine the final steady state obtained when multiple steady states exist. To characterize the flow, the terminology followed in the literature (see, for example, Moya and Ramos, 1987) is used. Flows which can develop from rest and uniform temperatures as initial conditions will be referred to as 'natural circulation' and those that circulate in a direction opposite to this will be called 'anti-natural circulation'. These terms are useful to help visualize possible flow modes associated with physically realizable situations. In addition, the terms 'symmetrical' and 'non-symmetrical' branches are used to describe identical flow fields but with counterclockwise and clockwise circulations. ψ_{ext} is positive for the former and negative for the latter.

Fig. 2 shows ψ_{ext} as a function of the Darcy–Rayleigh number obtained using Bi numbers from 0 to 5. The calculations were carried out for Rayleigh increasing from 0 to 100 and $Bi = 0$, using the initial conditions from the rest state. Other calculations were carried out for $Ra = 100 \rightarrow 0$ and $Bi = 0 \rightarrow 5$ using initial conditions from the solutions at higher Ra. By Eq. (14), the upper and lower branches correspond, respectively, to the counterclockwise (positive) and clockwise

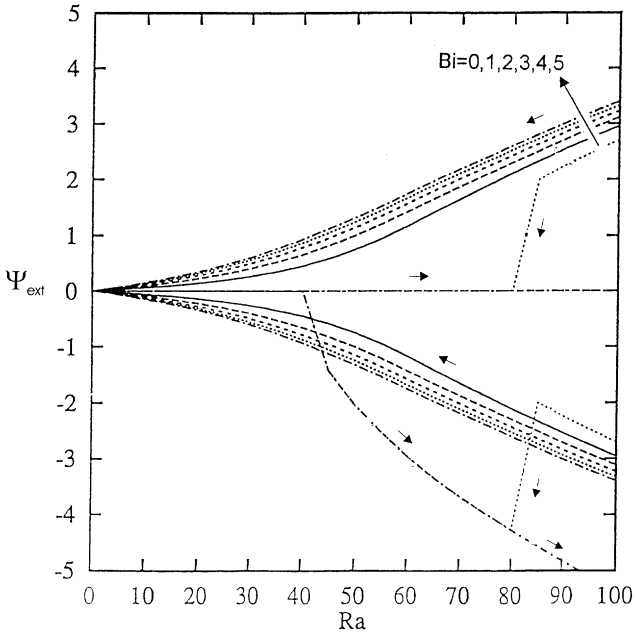

Fig. 2. ψ_{ext} as a function of the Darcy–Rayleigh number obtained using Bi numbers from 0 to 5.

(negative) motions. When increasing Ra from 0 to 100 and $Bi = 0$, a steady solution is obtained above $Ra = 4\pi^2$ until the final value of Ra. When decreasing Ra from 100 to 0 and $Bi = 1 \rightarrow 5$, two symmetric steady solutions are obtained and the flows are stable. For $Bi = 0$, the flow only remains stable until $Ra = 80$.

Similarly, ψ_{ext} as a function of the Darcy–Rayleigh number and for $Bi = 0$, 0.5 and 1 and Ra from 100 to 0 was obtained using initial conditions from the steady-state solutions at higher Ra. For $Bi = 1$, the initial condition was with a bicellular flow in the cavity, all the others with unicellular flows. It was seen that for $Bi = 1$, symmetrical upper and lower branches were obtained; for the others with $Bi = 0$ and 0.5, non-symmetric, steady solutions were obtained. A similar case is shown in Fig. 3 where the initial conditions for all the cases were from the steady-state solutions obtained at $Ra = 400$, $Bi = 0$ with unicellular flow. In this case, symmetrical upper and lower branches are obtained for $Bi = 0.8 \rightarrow 1.1$ and non-symmetric steady solutions for $Bi = 0 \rightarrow 0.7$. When the same case at $Ra = 0 \rightarrow 400$ was examined, it was seen that oscillating unicellular flows were observed for $Bi = 0$ and 0.1 at $Ra = 400$–360 range, which did not exist at lower Ra (see Fig. 4 which has the same initial condition as that of Fig. 3). The solutions at $Ra \simeq 360$ became unstable with respect to oscillatory disturbances and steady or sustained oscillating state later on. A cross plot of ψ_{ext} as a function of Bi with $Ra = 50$, 100, 300, 400 as a parameter showed that when increasing Ra from zero upward to the parametric values, the steady flow was obtained at $Bi = 0.5$ for $Ra = 50$, at $Bi = 0.7$ for $Ra = 100$, $Bi = 0.2$ for $Ra = 300$ and $Bi = 0.1$ for $Ra = 400$. When decreasing Ra from the parametric value down to zero, stable solutions were obtained for $Bi \geqslant 0.5$. ψ_{ext} as a function of time for the case of $Ra = 400$ and $Bi = 0$ was also examined and is shown in Fig. 5. The initial condition was a unicellular flow with $Ra = 100$. It is seen that the amplitude and the frequency

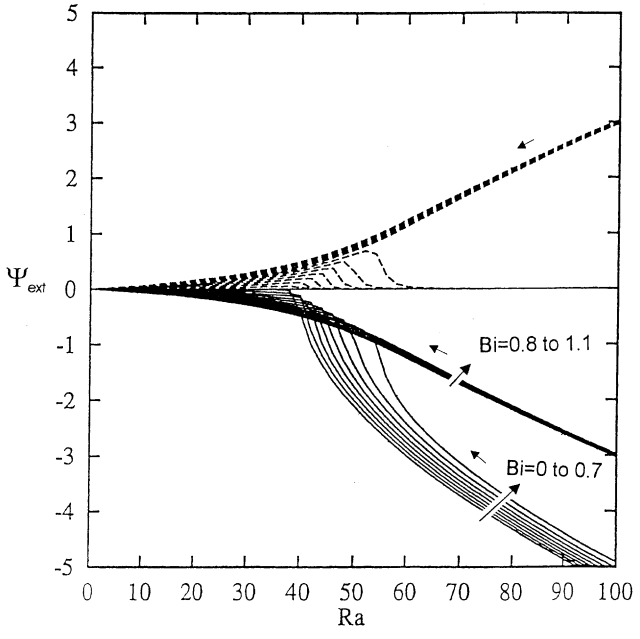

Fig. 3. ψ_{ext} as a function of the Darcy–Rayleigh number and various Bi numbers at the decreasing branch. The initial conditions for all the cases are from the steady-state solutions obtained at $Ra = 400, Bi = 0$ with unicellular flow. The symmetrical upper and lower branches are with Bi 0.8 → 1.1. Non-symmetrical upper and lower branches are for $Bi = 0 \rightarrow 0.7$.

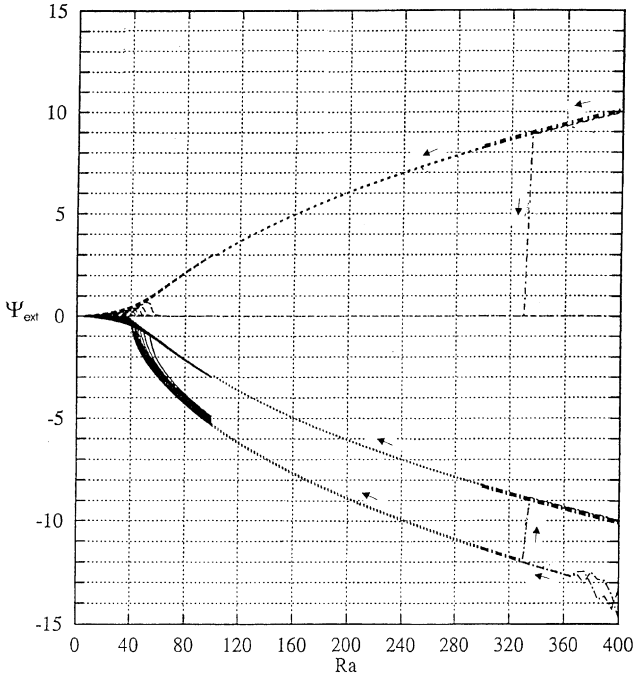

Fig. 4. ψ_{ext} as a function of the Darcy–Rayleigh number and various Bi numbers at the lower branch. The initial conditions are the same as for Fig. 3.

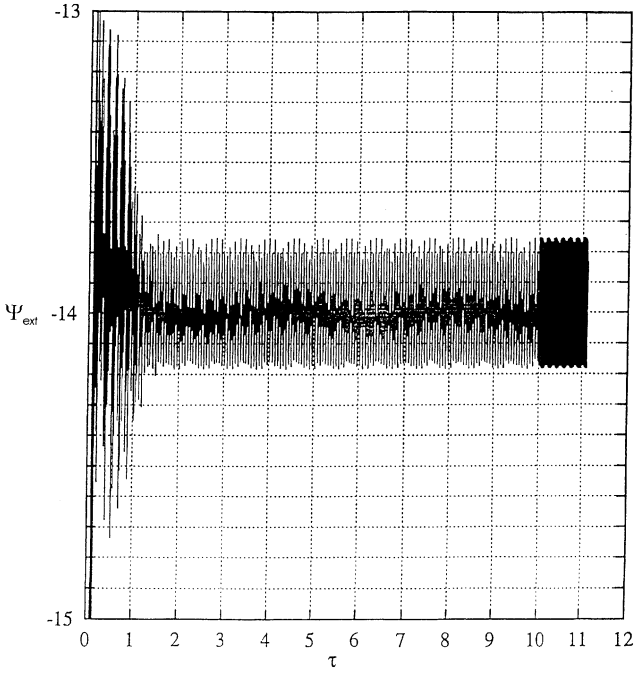

Fig. 5. ψ_{ext} as a function of time for the case of $Ra = 400$ and $Bi = 0$. The initial condition is with $Ra = 100$ and unicellular flow.

of oscillations are constant when the dimensionless time becomes greater than one and it is only one single frequency.

ψ_{ext} as a function of Bi from zero to 1.1 is shown in Fig. 6, where Ra is a variable parameter. The initial conditions are all anti-natural flows and are: (a) $Ra = 100$ and $Bi = 0$, (b) $Ra = 100$ and $Bi = 0.2$ and (c) $Ra = 250$ and $Bi = 0$. It is seen that the upper and lower branches are symmetrical for (a) and

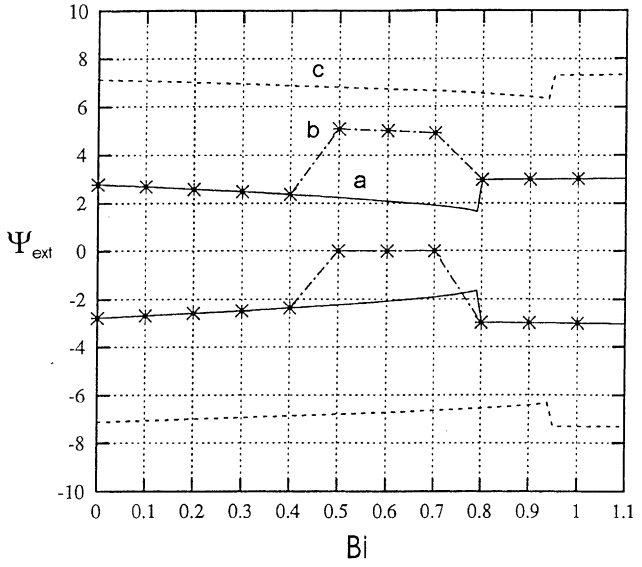

Fig. 6. ψ_{ext} as a function of Bi with Ra as a variable parameter for the case of $A=1$. Initial conditions are: (a) $Ra=100$ and $Bi=0$, (b) $Ra=100$ and $Bi=0.2$, and (c) $Ra=250$ and $Bi=0$.

(c). For case (b), the flow is bicellular anti-natural when $0 \leqslant Bi \leqslant 0.4$, unicellular natural when $0.4 \leqslant Bi \leqslant 0.8$ and bicellular natural when $Bi \geqslant 0.8$. For the case (c), similarly, it is bicellular anti-natural when $Bi \leqslant 0.95$ and bicellular natural when $Bi \geqslant 0.95$. Hence, there is a transition from anti-natural to natural flow around $Bi \simeq 0.95$. This phenomenon can be examined by plotting the streamlines and isotherms. Fig. 7 shows the streamlines (solid lines) and the isotherms (dash-dot lines) for this case where $Ra = 250$ and $Bi = 0 \rightarrow 1.1$. The solutions for $Bi = 0 \rightarrow 0.9375$ are anti-natural and for $Bi = 0.95$ there is a transition from the anti-natural to natural circulation. For $Bi = 0.975 \rightarrow 1.1$ they are all natural circulations. The isotherms show that as Bi increases from 0 to 0.9375, the temperature gradient in the vertical direction decreases and when $Bi = 0.95$, as the transition occurs from anti-natural to natural circulation, the isotherms become almost a mirror image of those at $Bi = 0.9375$. The streamlines show a similar trend.

To examine further the evolution of flow from anti-natural to natural, the streamlines (a) and isotherms (b) with time, τ from 2.56 to 3.50 are presented in Fig. 8 for the case of $Ra = 250$, $Bi = 0.95$. The initial conditions are from an anti-natural flow with $Ra = 250$, $Bi = 0$. The evolution from the anti-natural flow to that natural is noted at $\tau \geqslant 2.70$. The streamlines show that at $\tau = 2.56$, there are four cells, the main two in the center in an anti-natural circulation. As τ increases, first, the two side cells become equally important as the center cells, then, the side cells dominate the flow field with natural circulation at $\tau \geqslant 2.70$. Similarly for isotherms on the right-hand side: the change of isotherms in the center from $\tau = 2.66$ to 2.70 shows clearly how the energy transport shifts from two sides to the center.

The evolutions of ψ_{max}, ψ_{min} and Nu as a function of time ($\tau = 0 \rightarrow 3.5$) were also examined for the case of Fig. 8. The results are shown in Fig. 9, ψ_{ext}, Nu at the top and bottom and Nu at the left and right walls presented at (a), (b) and (c), respectively. The initial conditions are the same as of Fig. 8, from an anti-natural flow with $Ra = 250$ and $Bi = 0$. Fig. 9(a) shows clearly the evolution of ψ_{ext}, from the anti-natural to natural flow at $\tau \geqslant 2.70$. Fig. 9(b) shows the evolution of heat transfer Nu at the top and bottom of the cavity, while Fig. 9(c)

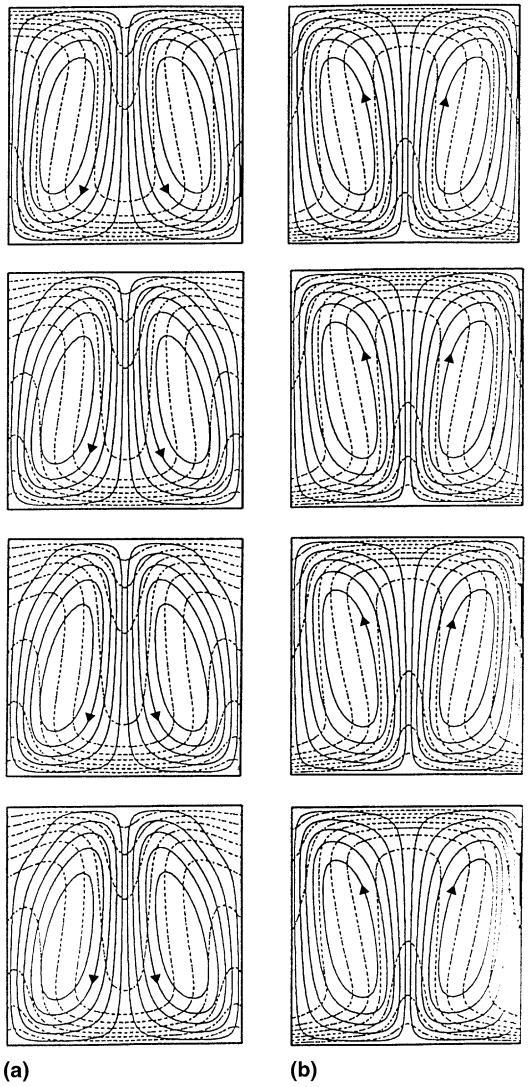

Fig. 7. (a) Streamlines (solid lines) and (b) the isotherms (dash-dot lines) for the case of $A = 1$, $Ra = 250$ and variable $Bi = 0 \rightarrow 1.1$. At the left, it is the case for anti-natural solution ($Bi=0$, 0.9, 0.925 and 0.9375 from top to bottom) and at the right, natural solution ($Bi=0.95$, 0.975, 1.0, 1.1 from top to bottom).

that at the lateral walls. It is seen that as expected, Nu at the top and bottom increases as the flow becomes with natural circulation carrying heat from the bottom to the top more effectively, and at the same time, Nu at the lateral walls decreases.

Similar results were obtained for the case of $Ra = 100$, $Bi = 0.8$ using initial conditions from an anti-natural flow with $Ra = 100$ and $Bi = 0$. The evolutions of ψ_{max}, ψ_{min} and Nu at bottom, top and side walls as a function of time ($\tau = 0 \rightarrow 7.0$) showed that the transition from the anti-natural to natural flow occurred at $\tau \geqslant 3.30$ with similar observations regarding ψ_{ext} and Nu.

To see the effect of various $Bi = 0.1 \rightarrow 1.0$ on the flow as a function of Ra, ψ_{ext} was calculated, and is shown in Fig. 10. The initial conditions are from the steady-state solutions obtained for $Ra = 250$, $Bi = 0$ and anti-natural bicellular flow. Solutions at upper and lower branches were all obtained with $250 \rightarrow 0$. For $Bi = 0.1$, the upper and lower branches are non-symmetric, and steady state for $Ra \geqslant 40$ and 70, respectively.

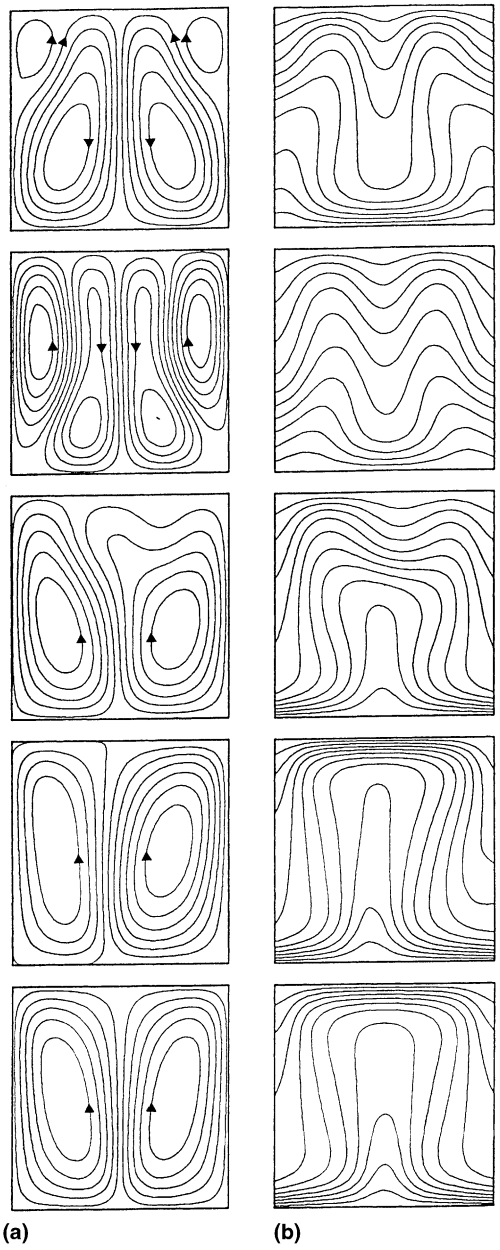

Fig. 8. (a) Streamlines and (b) isotherms for the case of $Ra = 250$, $Bi = 0.95$ with time, from 2.56 to 3.50 ($\tau = 2.56$, 2.66, 2.70, 2.72 and 3.50 from top to bottom).

For upper branch, $70 \leqslant Ra \leqslant 80$, the flow becomes unicellular and $Ra \geqslant 80$ anti-natural circulating two cells. For lower branch, $70 \leqslant Ra \leqslant 80$, the flow is unicellular and for $Ra \geqslant 80$, bicellular anti-natural circulation. For $Bi = 0.2$, a similar observation is made, with steady state unicellular flow at $Ra \geqslant 40$ and 60 at lower and upper branches, respectively. They are non-symmetric: For example at the upper branch, for $60 \leqslant Ra \leqslant 70$ unicellular anti-natural circulation and for $Ra \geqslant 80$ it is bicellular anti-natural circulation. For $Bi = 0.5$ the upper and lower branches are symmetrical and identical. For $Bi = 1.0$, it is noticed that the solutions at upper and lower branches are also the same and are symmetric. To confirm the observations made, the streamlines and isotherms were traced for each Bi. For example, the streamlines (solid lines) and isotherms (dash-dot lines) for the case of $Bi = 0.1$, anti-natural

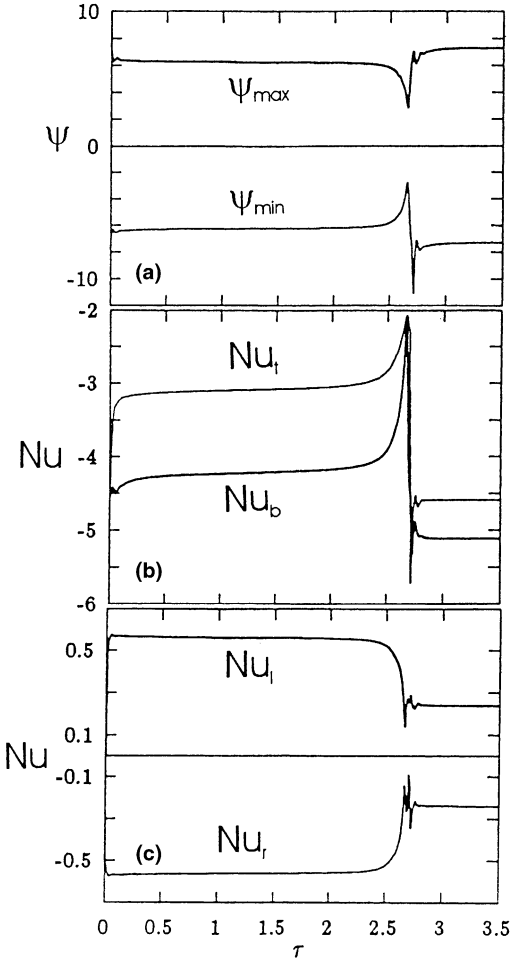

Fig. 9. Evolutions of ψ_{max}, ψ_{min} (a), and Nu at the top and bottom (b), Nu at the lateral walls (c) as a function of time ($\tau = 0 \rightarrow 3.5$) for the case of $A = 1$, $Bi = 0.95$, which is the same case of Fig. 6.

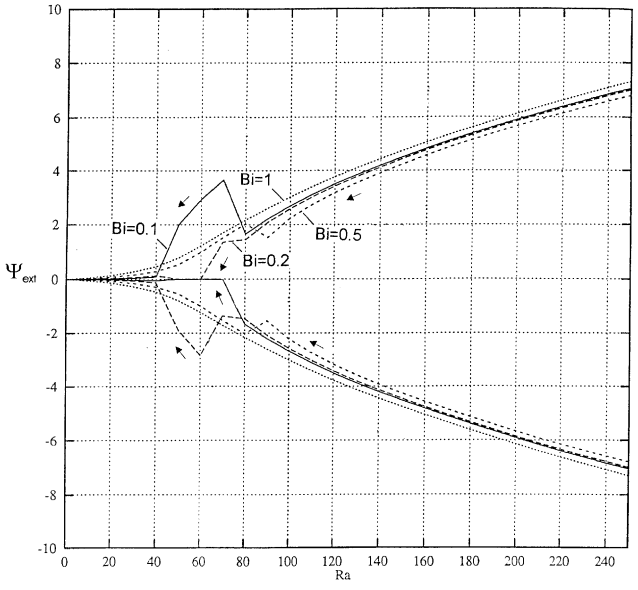

Fig. 10. ψ_{ext} as a function of Ra for the case of $A = 1$ and various $Bi = 0.1 \rightarrow 1.0$.

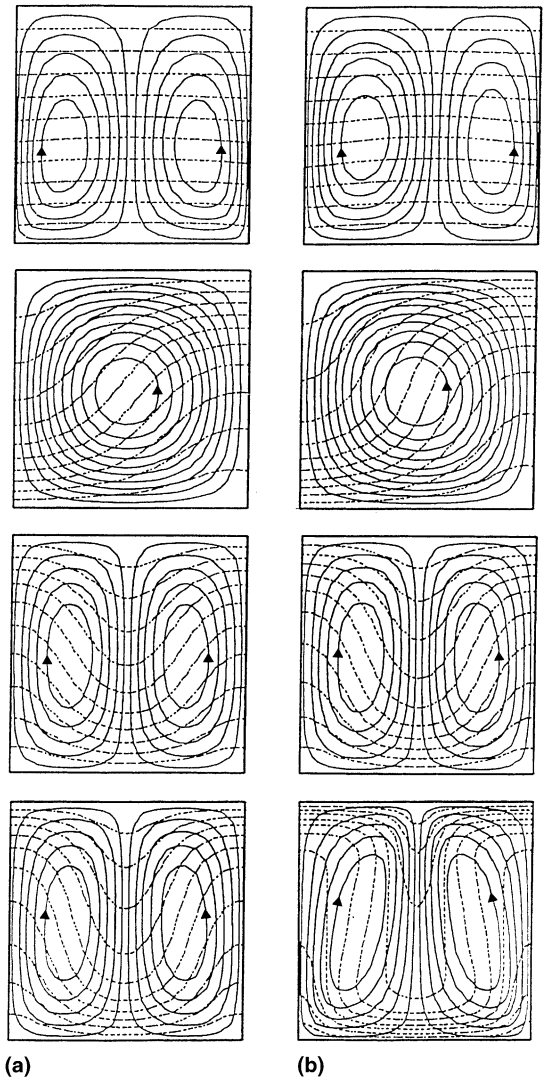

Fig. 11. (a) Streamlines (solid) and (b) isotherms (dash–dot) for the case of $Bi = 0.1$, anti-natural circulation at various $Ra = 20 \rightarrow 250$ (starting at the top, from left to right: $Ra = 20$, 40; $Ra = 50$, 60; $Ra = 80$, 90 and $Ra = 100$, 250).

flow at various $Ra = 20 \rightarrow 250$ are shown in Fig. 11(a) and (b). It is seen that following the observations made with Fig. 10, the flow is bicellular, anti-natural for low Ra numbers; for $Ra \geqslant 40$, the flow becomes unicellular and for $Ra \geqslant 80$ it becomes bicellular and anti-natural flow. Similar corroborating observations were also made for the other cases presented and discussed with Fig. 10.

Fig. 12 shows ψ_{ext} as a function of Ra from 0 to 500 for the case of $A = 1$ and $Bi = 0$ and 1. The initial conditions are from the steady-state solutions obtained for $Ra = 500$, $Bi = 0$ and bicellular anti-natural flow case. Solutions are obtained with $Ra = 0 \rightarrow 500$ and $Ra = 500 \rightarrow 0$, $Bi = 0$ and 1. For $Ra = 500 \rightarrow 0$ and $Bi = 1$, upper and lower branches are symmetric, for $Ra \leqslant 260$, it is bicellular anti-natural circulation, for $260 < Ra < 270$ it is unicellular anti-natural and for $Ra \geqslant 270$ it is natural circulating four cells. For $Ra = 0 \rightarrow 500$ and $Bi = 1$, upper and lower branches are also symmetric with anti-natural circulating two cells. For $Ra = 500 \rightarrow 0$ and $Bi = 0$, upper and lower branches are non-symmetric and steady state for $Ra \geqslant 40$ and 70, respectively. They become anti-natural circulating two cells at $Ra \geqslant 80$ and 70, respectively. For $Ra = 0 \rightarrow 500$ and $Bi = 0$, at $Ra \geqslant 40$, natural circulating two cells exist. At $Ra > 440$, an oscillation is noted.

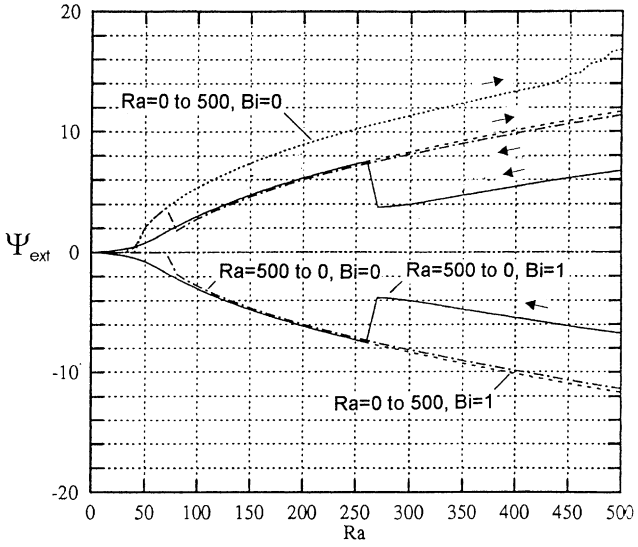

Fig. 12. ψ_{ext} as a function of Ra from 0 to 500 for the case of $A = 1$ and $Bi = 0$ and 1.

5. Conclusions

The development of Bénard cells is studied in a fluid-saturated porous enclosure whose bottom (warm) and top (cold) walls are isothermal and its vertical end walls are cooled. The results are analyzed in terms of the Darcy–Rayleigh number Ra, the Biot number Bi and the initial conditions. The results show that two branches exist that are related to the Darcy–Rayleigh and Biot numbers. The fluid remains stationary below a certain value of the Darcy–Rayleigh number. Two convective solution branches bifurcate from the zero solution in the direction of increasing Ra. If Ra is increased further, the solutions at $Ra \simeq 390$ become unstable with respect to oscillatory disturbances.

Acknowledgements

Financial support by Natural Sciences and Engineering Research Council of Canada is acknowledged.

References

Bau, H.H., Torrance, K.E., 1981. On the stability and flow reversal of an asymmetrically heated open convection loop. J. Fluid Mech. 106, 417–433.

Bories, S., 1970. Sur les Mécanismes Fondamentaux de la Convection Naturelle en Milieux Poreux, R.G.T. No. 108.

Caltagirone, J.P., Meyer, G., Mojtabi, A., 1981. Structurations thermoconvectives tridimensionnelles dans une couche poreuse horizontale. J. de Mécanique 20 (2), 219–232.

Caltagirone, J.P., Fabrie, H., 1989. Natural convection in a porous medium at high Rayleigh numbers. Part I – Darcy's model. Eur. J. Mech., B/Fluids 8, 207–227.

Caltagirone, J.P., 1975. Thermoconvective instabilities in a horizontal porous layer. J. Fluid Mech. 72 (2), 269–287.

Combarnous, M., 1970. Convection naturelle et convection mixte dans une couche poreuse horizontale. Rev. Gen. Therm. 9 (108), 1355–1375.

Combarnous, M., Bories, S., 1975. Hydrothermal convection in saturated porous media. Adv. Hydrosci. 10, 231–307.

Cheng, P., 1978. Heat transfer in geothermal systems. Adv. Heat Transfer 14, 1–105.

Graham, M.D., Steen, P.H., 1994. Plume formation and resonant bifurcations in porous-media convection. J. Fluid Mech. 272, 67–89.

Horne, R.N., O'Sullivan, M.J., 1974. Oscillatory convection in a porous medium heated from below. J. Fluid Mech. 66 (2), 339–352.

Horne, R.N., O'Sullivan, M.J., 1978. Origin of oscillatory convection in a porous medium heated from below. Phys. Fluids 21 (8), 1260–1264.

Moya, S.L., Ramos, E., 1987. Numerical study of natural convection in a tilted rectangular porous material. Int. J. Heat Mass Transfer 30 (4), 741–756.

Mukutmoni, D., Yang, K.T., 1995. Thermal convection in small enclosures: an a typical bifurcation sequence. Int. J. Heat Mass Transfer 38 (1), 113–126.

Roache, P.J., 1982. Computational Fluid Dynamics. Hermosa Publishers, Albuquerque, NM.

Schubert, G., Straus, J.M., 1979. Three-dimensional and multicellular steady and unsteady convection in fluid-saturated porous media at high Rayleigh numbers. J. Fluid Mech. 94, part 1, 25–38.

Zhang, X., 1992. Natural convection in an inclined water-saturated porous cavity: the duality of solutions. Heat and Mass Transfer in Porous Media ASME HTD-Vol. 216.